Angewandte Chemie International Edition

Angewandte International Edition Chemie

How to cite: *Angew. Chem. Int. Ed.* **2026**, e3983956
doi.org/10.1002/anie.3983956

COMMUNICATION

Near-100% Selective Photocatalytic Methane-to-Methanol Conversion Enabled by Synergistic Chlorine Radicals and Oxygen Vacancies

Guang-Xing Dong[1,2] | Min Zhang[1,2] | Ting Zheng[2] | You-Xiang Feng[2] | Meng-Ran Zhang[2] | Su-Xian Yuan[2] | Lianqi Zhang[1,2] | Tong-Bu Lu[1,2]

[1]State Key Laboratory of Crystal Materials, Tianjin Key Laboratory of Functional Crystal Materials, Institute of Functional Crystals, Tianjin University of Technology, Tianjin, China | [2]Institute For New Energy Materials and Low Carbon Technologies, School of Electrical Engineering and Automation, Tianjin University of Technology, Tianjin, China

Correspondence: Min Zhang (zm2016@email.tjut.edu.cn) | Lianqi Zhang (tianjinzhanglq@163.com) | Tong-Bu Lu (lutongbu@tjut.edu.cn)

Received: 20 January 2026 | **Revised:** 20 April 2026 | **Accepted:** 8 May 2026

Keywords: C—H activation | CH_4 conversion | Cl•-mediated selective oxidation | photocatalysis | radical/active-site synergistic

ABSTRACT

The selective photocatalytic conversion of methane to a single product is a grand challenge, primarily due to uncontrollable over-oxidation and inefficient reduction. Herein, we pioneer a radical/active-site synergistic strategy to steer the reaction pathway exclusively toward methanol. This is realized by a dual-functional Cl—TiO_2-OV catalyst that integrates chlorine modification and oxygen vacancy (OV) engineering. Crucially, surface chlorine redirects the oxidation route: instead of generating non-selective •OH radicals from H_2O, photogenerated holes preferentially drive a $Cl^-/Cl•$ cycle. The resulting Cl• radicals activate the C—H bond of CH_4 to form $•CH_3$, which combines with O_2 to yield the CH_3OOH intermediate. Simultaneously, the engineered OV sites act as electron-rich centers that efficiently reduce CH_3OOH to CH_3OH. This decoupling of selective oxidation (via Cl•) and efficient reduction (via OVs) suppresses all side-reactions, delivering methanol with nearly 100% selectivity and a yield of 1242 μmol g^{-1}. In contrast, TiO_2-OV suffers from •OH-mediated sequential oxidation to $HCHO/CO_2$, and Cl—TiO_2 lacks sufficient reduction power, resulting in a CH_3OOH/CH_3OH mixture. This work not only offers an effective approach for highly selective photocatalytic methane conversion but also deepens mechanistic insight into radical/active-site cooperativity in synergistic catalysis.

Natural gas has become a pivotal energy source in the 21st century due to its abundant reserves and low cost. However, its principal component, methane, possesses a global warming potential far exceeding that of CO_2 [1–3]. The efficient conversion of methane into high-value chemicals under mild conditions could thus deliver integrated benefits, including enhanced energy utilization, economic gain, and environmental protection [4–6]. In this context, photocatalytic methane conversion is regarded as a promising green technology, as it can circumvent the limitations of conventional thermal catalysis, such as high temperature, high pressure, and substantial energy consumption [7–14]. In recent years, considerable progress has been achieved, with various photocatalysts enabling the transformation of methane into high-value products such as CH_3OH, HCHO, CH_3OOH, C_2H_6, and C_2H_5OH [15–26]. The key step universally lies in the initial activation of the inert C—H bond, which is often achieved by highly oxidizing species, such as photogenerated holes (h^+) or hydroxyl radicals (•OH) [27–31]. Nonetheless, this strategy presents a fundamental dilemma: the same high reactivity required to cleave the strong C—H bond often leads to uncontrollable sequential over-oxidation of the desired intermediates, yielding complex mixtures of C_1 oxygenates [32–35]. Furthermore, inefficient reduction

© 2026 Wiley-VCH GmbH

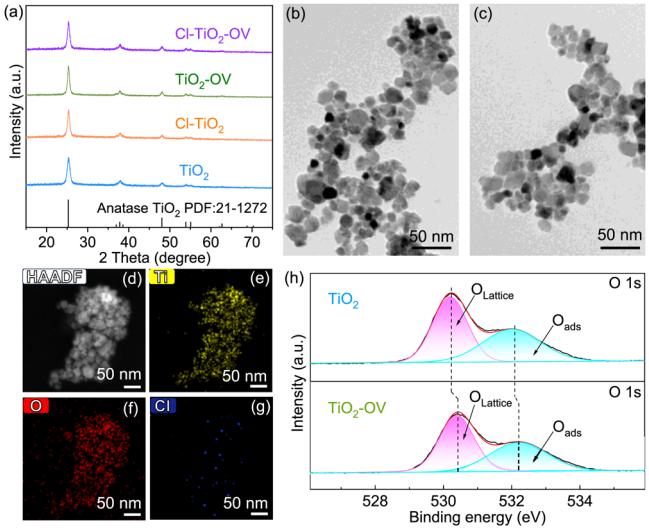

FIGURE 1 | (a) XRD patterns of various photocatalysts. TEM images of (b) TiO_2-OV and (c) Cl—TiO_2-OV. (d) HAADF-TEM image of Cl—TiO_2-OV. EDS mapping images of (e) Ti, (f) O, and (g) Cl in Cl—TiO_2-OV. (h) XPS spectra of O 1s in TiO_2 and TiO_2-OV.

kinetics impede the complete and selective transformation of these intermediates into a single target product. Consequently, achieving highly selective photocatalytic conversion of methane to a single product remains a formidable, yet critical, challenge.

To address the selectivity challenge, we propose a radical/active-site synergistic strategy designed to modulate the C—H activation pathway and accelerate reduction kinetics. This strategy is implemented in a dual-functional Cl—TiO_2-OV catalyst, constructed by integrating chlorine modification with oxygen vacancy (OV) engineering. In this system, surface Cl^- ions are preferentially oxidized by photogenerated holes to generate Cl• radicals, which efficiently cleave the C—H bonds of methane to form $•CH_3$ radicals. These intermediates subsequently react with O_2 and undergo protonation, forming a CH_3OOH species, which is then rapidly reduced to CH_3OH at the electron-rich OV sites. The Cl•-mediated activation suppresses over-oxidation, while the electron-rich OV sites accelerate the reduction kinetics and promote the complete conversion of the CH_3OOH intermediate. These cooperative effects lead to near-100% selectivity toward methanol, with minimal formation of by-product or CO_2. In contrast, OV-rich TiO_2 (TiO_2-OV) follows a conventional •OH-dominated sequential oxidation pathway, yielding methanol with only 66.5% selectivity alongside over-oxidation by-products (HCHO and CO_2). Meanwhile, chlorine-modified TiO_2 (Cl—TiO_2) alone, which lacks OV sites, exhibits sluggish reduction kinetics and produces a mixture of CH_3OOH and CH_3OH.

Pristine TiO_2 was synthesized via a reported solvothermal method [36], followed by chlorination via impregnation in concentrated HCl to generate Cl-TiO_2 [37], or by annealing under Ar to generate TiO_2-OV. The dual-functional Cl—TiO_2-OV catalyst was constructed via sequential OV engineering and chlorination (see details in the supporting information). The x-ray diffraction (XRD) patterns confirm that all samples retain the anatase phase without structural alteration (Figure 1a). Transmission electron microscopy (TEM) images further reveal that all samples exhibit nanosheet morphology with an average size of 20–25 nm, atomic force microscopy (AFM) characterization shows an average nanosheet thickness of 3.6 nm (Figures 1b,c, S1, and S2), indicating that neither OV creation nor chlorination alters the crystalline structure or morphology of TiO_2. High-resolution TEM (HRTEM) analysis revealed a lattice spacing of 3.5 Å, corresponding to the (101) plane of anatase TiO_2 (Figure S3). Energy-dispersive x-ray spectroscopy (EDS) elemental mapping and energy spectrum further confirm the homogeneous distribution of Ti, O, and Cl elements on the surface of Cl—TiO_2-OV (Figures 1d–g, S4, and S5), verifying successful dual-functionalization. X-ray photoelectron spectroscopy (XPS) analysis further revealed that the Cl 2p spectra of Cl-TiO_2 and Cl—TiO_2-OV display two peaks at 198.02 and 199.61 eV (Figure S6), with the peak at 198.02 eV attributable to the formation of Ti—Cl bonds. FTIR spectroscopy further detects Ti—Cl bonds in the chlorinated samples. Ion chromatography reveals chlorine contents of 0.69 and 0.81 wt.% for Cl—TiO_2 and Cl—TiO_2-OV, respectively, confirming surface chlorination (Figures S7 and S8). Concurrently, the O 1s spectra (Figure S9) of TiO_2 and Cl—TiO_2 exhibit two distinct components: lattice oxygen at lower binding energy and surface-adsorbed oxygen at higher binding energy. Notably, Cl—TiO_2 exhibits a marked decrease in the adsorbed oxygen signal compared to pristine TiO_2 (Figure S4), suggesting a substitution reaction wherein Cl^- replaces surface oxygen species [38, 39]. TiO_2-OV shows a positive shift (0.18 eV) in the $O_{Lattice}$ 1s binding energy relative to TiO_2 (Figures 1h and S10), consistent with OV formation due to its electron-withdrawing effect [40, 41].

The formation of OVs was further corroborated by electron paramagnetic resonance (EPR) spectroscopy. As shown in Figure 2a, a pronounced symmetric signal at $g = 2.003$ was observed for both Cl—TiO_2-OV and TiO_2-OV. Notably, Cl—TiO_2 also exhibited a signal indicative of limited OV formation, suggesting that chlorination can generate a small number of OVs, consistent with prior reports [37], and the calculated oxygen vacancy content agrees well with the EPR measurement results (Table S1). UV–vis diffuse reflectance spectra (DRS) show a slight redshift and enhanced visible-light absorption (400–500 nm) for OV-containing samples (Figure 2b), attributed to the introduction of OVs [42]. Mott–Schottky plots indicate that Cl—TiO_2-OV and TiO_2-OV possess a higher charge-carrier density than pristine TiO_2, as reflected by their reduced slopes (Figure 2c). This enhancement is ascribed to abundant surface OVs, which promote charge separation [36, 43]. Transient photocurrent responses and electrochemical impedance spectroscopy (EIS) measurements (Figures S11 and S12) further validated the enhanced charge kinetics in OV-containing samples. The quenching of the 2,2,6,6-tetramethylpiperidinooxy (TEMPO) EPR signal, an indicator of photogenerated electron density [44], is significantly stronger for OV-containing catalysts than for TiO_2 (Figure 2d), directly verifying the role of OVs in boosting charge carrier generation. Surface photovoltage (SPV) measurements under illumination revealed that Cl—TiO_2-OV exhibits a significantly larger SPV average amplitude (81.1 mV) than Cl—TiO_2 (38.3 mV) (Figure 2e,f), indicating a higher accumulation of photogenerated electrons at the surface and further demonstrating that the presence of OV effectively promotes charge separation and transport.

To circumvent the low aqueous solubility of methane, photocatalytic performance was assessed in a gas–solid system at

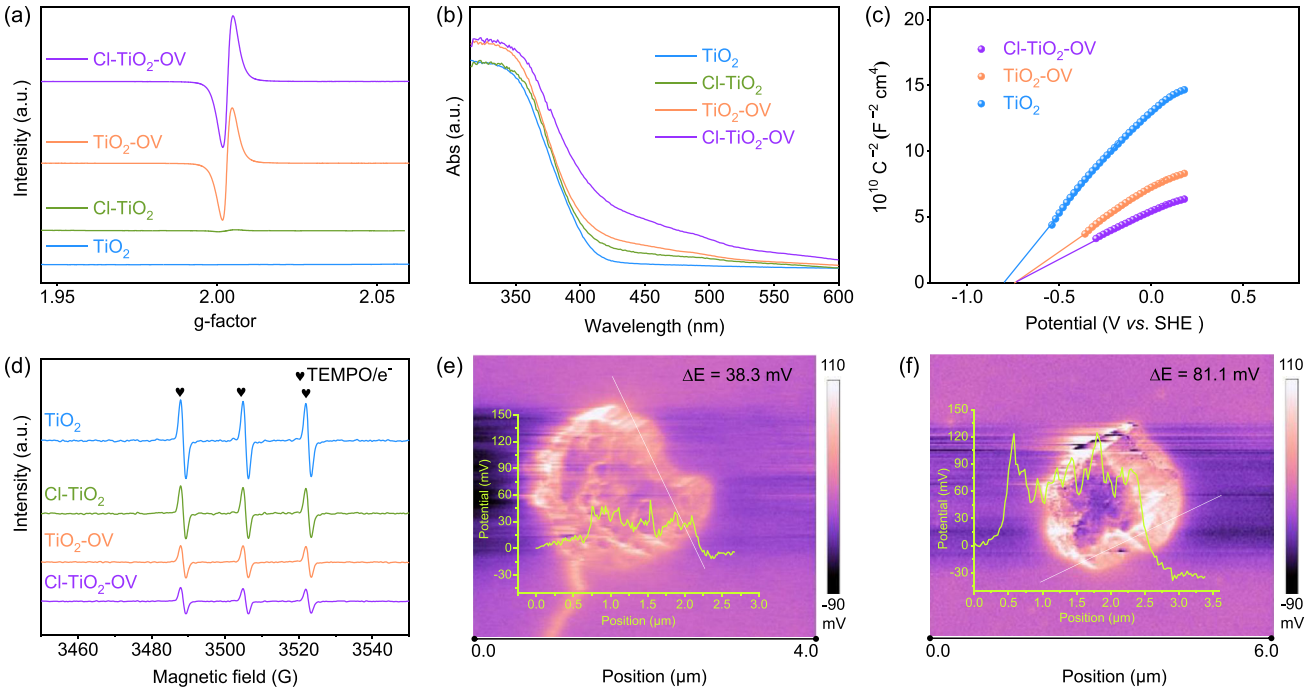

FIGURE 2 | (a) EPR spectra, (b) UV–vis DRS spectra, and (c) Mott–Schottky curves of various photocatalysts. (d) EPR spectra of various photocatalyst suspensions with TEMPO under irradiation. KPFM images and the corresponding surface potential profiles with 365 nm UV light illumination of (e) Cl—TiO_2 and (f) Cl—TiO_2-OV, ΔE represents the average amplitude of surface photovoltage.

atmospheric pressure (Figure S13). As shown in Figure 3a (top), pristine TiO_2 and TiO_2-OV primarily produced CH_3OH and HCHO, along with the over-oxidation product CO_2. While TiO_2-OV exhibits enhanced activity due to improved charge separation, its CH_3OH selectivity remained limited to 66.5%. In stark contrast, for the chlorinated Cl—TiO_2 catalyst, CH_3OOH emerged as the main by-product, with neither CO_2 nor HCHO detected, demonstrating effective suppression of over-oxidation. However, the selectivity towards CH_3OH was only 59.8%. Remarkably, the dual-modified Cl—TiO_2-OV catalyst achieved nearly-100% selectivity for CH_3OH with a yield of 1242 μmol g^{-1}, and an apparent quantum yield (AQY) of 1.47% at 400 nm (Table S2), and virtually no by-products were observed (Figures S14–S18). Under similar mild conditions, the catalyst exhibits superior high selectivity toward the single product CH_3OH compared to previously reported catalysts (Table S3). This exclusive selectivity underscores the indispensable synergy between OVs and Cl modification in directing the reaction pathway toward a single desired product. Control experiments confirmed that the product originated from photocatalytic methane conversion over the catalyst. Continuous time-dependent photocatalytic activity evaluation and methanol oxidation control experiments demonstrated that the Cl—TiO_2-OV catalyst effectively suppresses overoxidation of the product to CO_2 in the methane conversion system, while maintaining stable and highly selective conversion to the single product CH_3OH (Figures S19–S22). Under anhydrous conditions (Figure 3a, bottom), photocatalytic methane activation over non-chlorinated catalysts (TiO_2 and TiO_2-OV) was nearly suppressed, underscoring the essential role of H_2O. Conversely, the chlorinated catalysts (Cl—TiO_2 and Cl—TiO_2-OV) maintained significant activity, demonstrating their unique capability for water-independent methane activation. Notably, HCHO formation in chlorinated systems is attributed to a condition-dependent bifurcation of the CH_3OOH intermediate: under optimal conditions with sufficient electrons and protons, CH_3OOH is preferentially reduced to CH_3OH; however, when electron/proton supply is limited, partial dehydration to HCHO occurs [45].

Radical-trapping experiments elucidated the origin of the selectivity divergence. For TiO_2-OV (Figure 3b), EPR studies revealed that $\bullet CH_3$ radicals are generated exclusively via hydrogen abstraction from CH_4 by •OH radicals, which themselves originate from H_2O oxidation by photogenerated holes. In sharp contrast, for chlorinated catalysts, a clear $\bullet CH_3$ signal was observed even in the absence of H_2O, with no detectable •OH radical (Figure 3c), unambiguously demonstrating a H_2O-independent $\bullet CH_3$ generation pathway. In all systems, subsequent introduction of O_2 immediately produced a $CH_3OO\bullet$ signal, confirming rapid formation of the key CH_3OOH intermediate. In situ Fourier-transform infrared (FTIR) spectroscopy further resolved the competing reaction pathways (Figure 3d,e). For TiO_2-OV, spectral evolution under illumination confirmed the concurrent formation of intermediates along the CH_3OH pathway (•OH (1655 cm^{-1}), $\bullet CH_3$ (1456 cm^{-1}), $CH_3O\bullet$ (1116 cm^{-1})) and those leading to over-oxidation products ($\bullet CH_2OH$ (1542 cm^{-1}), CHO• (1747 cm^{-1}) for HCHO; peroxidic $\bullet CO_2$ (1575 cm^{-1}), and HCOO• (1338 cm^{-1}) for CO_2 [46–48]. Conversely, for the Cl—TiO_2-OV system, produced only the key CH_3OH intermediates ($\bullet CH_3$ and $CH_3O\bullet$) were distinctly observed under standard conditions. The transient accumulation of CHO• (1747 cm^{-1}) only under strictly anhydrous conditions aligns with the minor HCHO formation, while no signals for deep-oxidation intermediates were detected, consistent with near-perfect selectivity.

Isotope labeling experiments using $^{18}O_2 + H_2{}^{16}O$ provided definitive evidence for the altered reaction pathways (Figures 4a–c,

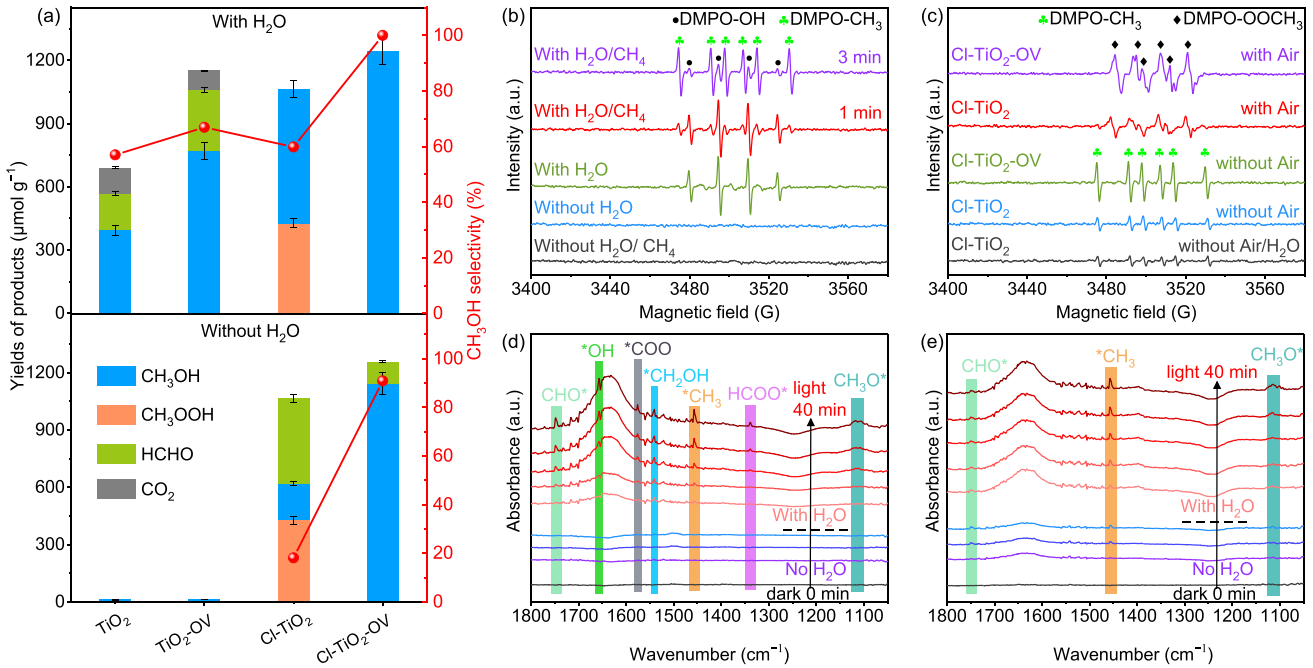

FIGURE 3 | (a) Product yields and CH_3OH selectivity using different photocatalysts with (top) or without (below) H_2O. CH_3OH selectivity was calculated as: selectivity = n(CH_3OH)/(n(CH_3OH) + n(CH_3OOH) + n(HCHO) + n(CO_2)), where n(CH_3OH), n(CH_3OOH), n(HCHO), and n(CO_2) represent their respective yields. (b) EPR spectra of DMPO-OH and DMPO-CH_3 under different reaction conditions with TiO_2-OV as photocatalyst. (c) EPR spectra of DMPO-CH_3 and DMPO-$OOCH_3$ under different reaction conditions with Cl—TiO_2 or Cl—TiO_2-OV as photocatalyst. In situ FTIR spectra of (d) TiO_2-OV and (e) Cl—TiO_2-OV under different light irradiation times before and after H_2O introduction.

S23, and S24). Non-chlorinated catalysts produced primarily $CH_3{}^{16}OH$ (m/z = 32, oxygen from H_2O) and $C^{16}O_2$ (m/z = 44, oxygen from H_2O), under an $^{18}O_2$ + $H_2{}^{16}O$ atmosphere, supporting an •OH-mediated consecutive oxidation mechanism (Figures 4a,b and S10). In stark contrast, the Cl—TiO_2-OV system produced almost exclusively $CH_3{}^{18}OH$ (m/z = 34, oxygen from O_2) accompanied by $H_2{}^{18}O$ (m/z = 20, oxygen from O_2), demonstrating a complete switch in the oxygen source (Figure 4a,c). These results conclusively indicate that methanol is formed via reductive dehydration of the CH_3OOH intermediate (CH_3OOH + $2H^+$ + $2e^-$ → CH_3OH + H_2O) in the chlorinated system, as opposed to the direct •OH/•CH_3 coupling dominant on TiO_2-OV. This is consistent with the observation that anhydrous and anoxic reaction conditions suppress the catalytic activity of non-chlorinated and chlorinated catalysts, respectively (Figures 3a bottom and S25).

To pinpoint the origin of the high CH_3OH selectivity, we directly probed the active chlorine species using molecular and radical trapping. ^{1}H NMR and EPR analyses confirmed the photogenerated-hole-driven oxidation of surface Cl^- to Cl• radicals during the reaction (Figures S26 and S27) [49, 50]. Concurrent fluorescence probing with coumarin detected •OH exclusively in the TiO_2-OV system (Figure S28) [51, 52], consistent with the earlier EPR results (Figure 3b), directly demonstrating that chlorine incorporation effectively suppresses •OH generation by redirecting hole oxidation. This critical shift replaces high reactive •OH with milder and more selective Cl• radicals for C—H activation, thereby suppressing the uncontrolled sequential oxidation pathways responsible for CO_2 and HCHO formation on TiO_2-OV. The complete conversion to CH_3OH is then enabled by the complementary reduction function. The engineered OVs in Cl—TiO_2-OV dramatically enhance electron-transfer kinetics, driving this reduction to completion. In contrast, Cl—TiO_2, which lacks sufficient OVs, exhibits sluggish reduction, resulting in a CH_3OH/CH_3OOH mixture.

A series of quenching experiments was performed to validate the distinct functions of holes, Cl• radicals, and electrons (Figure S29). Hole quenching with triethylamine (Et_3N) substantially suppresses the activity of all systems, confirming holes as essential drivers. Scavenging Cl• radicals with PBN strongly inhibited only Cl—TiO_2-OV, directly establishing Cl• as the indispensable active species in the chlorinated system. Electron quenching with $NaIO_3$ nearly eliminated CH_3OH formation in Cl-TiO_2-OV and led to CH_3OOH accumulation, verifying that CH_3OH originates from electron-mediated reductive dehydration of CH_3OOH. In contrast, TiO_2-OV still produced CH_3OH under the same conditions, supporting its direct •OH/•CH_3 coupling pathway. Post-reaction XPS, ion chromatography, FTIR spectroscopy, and cycling experiments confirmed the stability and recyclability of surface chlorine species (Figures S30–S33), evidencing an efficient chlorine cycle.

Integrating all evidence, we propose distinct yet interconnected methane conversion pathways for the single and dual-modified catalysts, summarized in Figures 4d and S34. (1) •OH-dominated sequential oxidation for TiO_2-OV system: Photogenerated holes oxidize H_2O to •OH, which activates CH_4 to •CH_3. While most •CH_3 couples directly with •OH to yield CH_3OH, the high reactivity of •OH also drives sequential over-oxidation to HCHO and CO_2. A minor fraction of •CH_3 forms CH_3OOH, which can be reduced at OV sites. (2) Cl•-mediated activation with limited reduction for Cl—TiO_2 system: The ionization energy (IE) of Cl^-

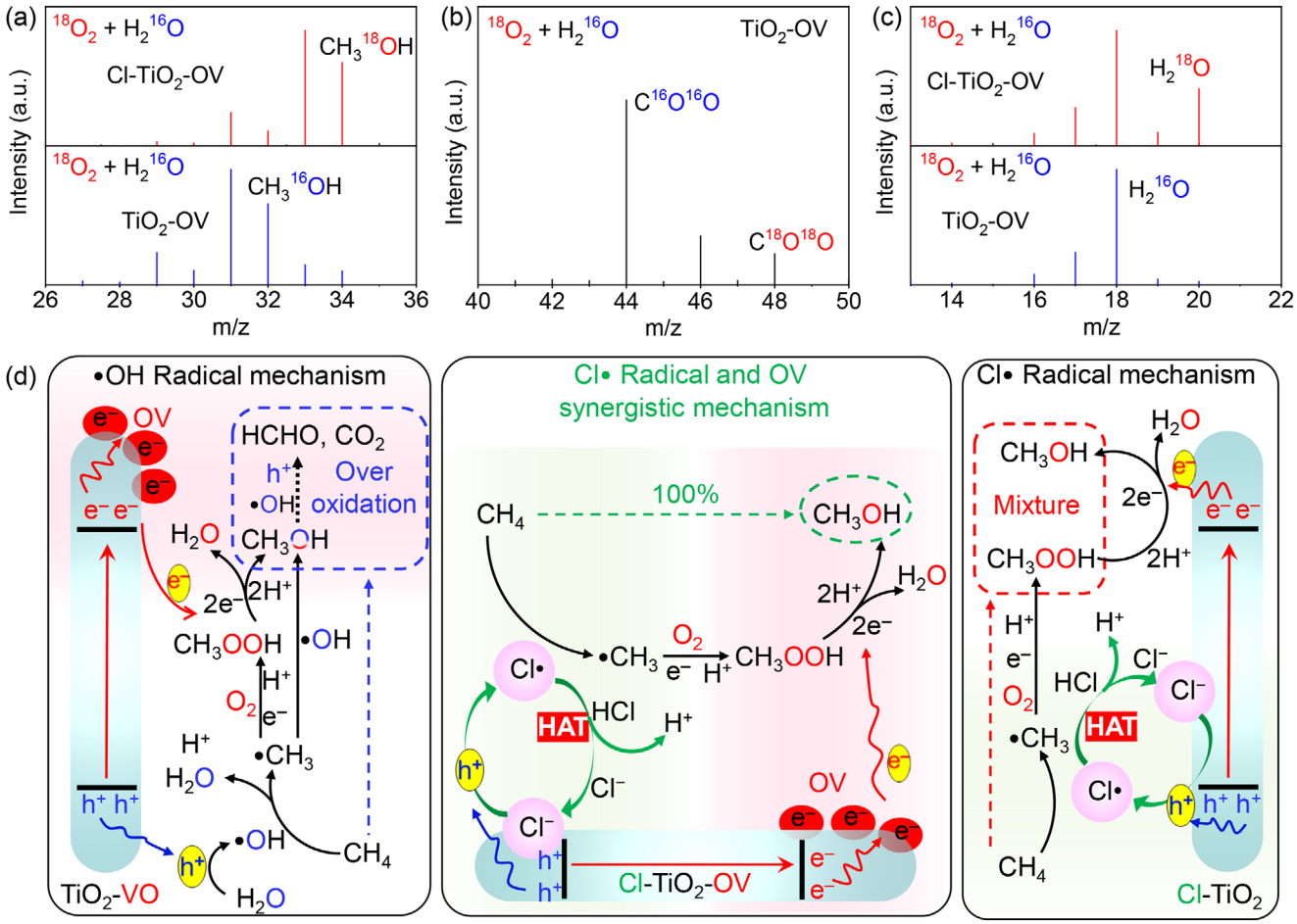

FIGURE 4 | Mass spectra of (a) CH_3OH, (b) CO_2, and (c) H_2O generated over TiO_2-OV or Cl—TiO_2-OV with $^{18}O_2 + H_2{}^{16}O$ as feedstocks. (d) Schematic diagram of the proposed reaction pathway for CH_4 conversion with TiO_2-OV, Cl—TiO_2, or Cl—TiO_2-OV as photocatalyst, HAT represents the hydrogen atom transfer.

($Cl^- \rightarrow Cl\bullet + e^-$; IE = 3.61 eV) is significantly lower than the first IE of H_2O ($H_2O \rightarrow H_2O^+ + e^-$, IE = 12.6 eV) [53, 54], indicating that Cl^- is thermodynamically favored for oxidation. Surface Cl^- preferentially scavenges photogenerated holes to generate Cl• radicals, which selectively activate the C—H bond of CH_4 via hydrogen atom transfer (HAT) ($Cl\bullet + CH_4 \rightarrow \bullet CH_3 + HCl$). Subsequently, Cl^- is re-adsorbed onto the catalyst surface, establishing a closed Cl^-/Cl• cycle. The resulting $\bullet CH_3$ forms CH_3OOH with O_2/protons. Due to insufficient reduction capability, CH_3OOH reduction is incomplete, leading to a CH_3OH/CH_3OOH mixture. A closed Cl^-/Cl• cycle prevents hole-mediated over-oxidation. (3) Synergistic Cl•/OV catalysis for Cl—TiO_2-OV system: This system integrates and optimizes both functions: chlorine directs oxidation via the selective Cl• pathway, completely suppressing •OH generation and its associated over-oxidation; meanwhile, abundant OVs dramatically enhance electron flux, enabling the complete and rapid reduction of CH_3OOH to CH_3OH. The synergy between Cl•-mediated selective oxidation and OV-facilitated efficient reduction constitutes the fundamental origin of the near-100% methanol selectivity.

In summary, we have developed a dual-functional Cl—TiO_2-OV catalyst that achieves near-perfect selectivity in the photocatalytic conversion of methane to methanol under mild conditions. Mechanistic studies revealed that chlorine modification and oxygen-vacancy engineering play distinct yet complementary roles: Chlorine not only suppresses •OH formation to inhibit over-oxidation but also generates selective Cl• radicals for methane activation. Meanwhile, oxygen vacancies markedly enhance electron reduction kinetics, ensuring the efficient conversion of the CH_3OOH intermediate to the target product. This work exemplifies how a synergistic radical/active-site strategy can unlock precise reaction control, providing a strategic blueprint for designing high-selectivity photocatalysts for methane upgrading.

Author Contributions

Guang-Xing Dong: writing – original draft, investigation, methodology. **Min Zhang**: conceptualization, supervision, project administration, writing – review and editing, funding acquisition. **Ting Zheng**: investigation. **You-Xiang Feng**: investigation. **Meng-Ran Zhang**: investigation. **Su-Xian Yuan**: investigation. **Lianqi Zhang**: funding acquisition, supervision, writing – review and editing. **Tong-Bu Lu**: supervision, writing – review and editing, funding acquisition.

Acknowledgments

This work was financially supported by the National Key R&D Program of China (2022YFA1502902), NSFC (22475152 and U21A20286), Tianjin

Natural Science Foundation Project (24JCYBJC00840), and the 111 Project of China (D17003).

Conflicts of Interest

The authors declare no conflicts of interest.

Data Availability Statement

The data that support the findings of this study are available from the corresponding author upon reasonable request.

References

1. J. Xie, C. Fu, M. G. Quesne, et al., "Methane Oxidation to Ethanol by a Molecular Junction Photocatalyst," *Nature* 639 (2025): 368–374, https://doi.org/10.1038/s41586-025-08630-x.

2. T. Ishizuka and T. Kojima, "Oxidative and Reductive Manipulation of C1 Resources by Bio-Inspired Molecular Catalysts to Produce Value-Added Chemicals," *Accounts of Chemical Research* 57 (2024): 2437–2447, https://doi.org/10.1021/acs.accounts.4c00390.

3. X. Wang, G. Jiang, X. He, et al., "A Broad Range of Aromatic Carboxylic Acids for Photocatalytic Methane Oxidation," *Advanced Materials* 37 (2025): 2504866, https://doi.org/10.1002/adma.202504866.

4. T. Zhong, X. Long, Z. Yao, et al., "High Value-added Conversion of Atmospheric Pollutants and Greenhouse Gases: Assessment of Bottlenecks and Optimization Strategies for Mainstream Catalytic Technology," *Journal of Cleaner Production* 521 (2025): 146145, https://doi.org/10.1016/j.jclepro.2025.146145.

5. Y. Xu, C. Wang, X. Li, et al., "Efficient Methane Oxidation to Formaldehyde via Photon–Phonon Cascade Catalysis," *Nature Sustainability* 7 (2024): 1171–1181, https://doi.org/10.1038/s41893-024-01401-y.

6. Y. Fan, Y. Jiang, H. Lin, et al., "Insight Into Selectivity of Photocatalytic Methane Oxidation to Formaldehyde on Tungsten Trioxide," *Nature Communications* 15 (2024): 4679, https://doi.org/10.1038/s41467-024-49138-8.

7. Y. Yuan, J. Zhou, A. Bayles, H. Robatjazi, P. Nordlander, and N. J. Halas, "Steam Methane Reforming Using a Regenerable Antenna–Reactor Plasmonic Photocatalyst," *Nature Catalysis* 7 (2024): 1339–1349, https://doi.org/10.1038/s41929-024-01248-8.

8. H. Tang, Y. Ma, C. Zhu, et al., "Highly Efficient Ambient Temperature Photo-oxidation of CH_4 to C1 Products Over CeO_2 Supported Single-Atom Fe With Oxygen Vacancies," *Journal of Materials Chemistry A* 12 (2024): 18604–18612, https://doi.org/10.1039/D4TA01284D.

9. H. Gong, L. Zhang, C. Deng, et al., "Selective Photocatalytic Aerobic Oxidation of Methane to Methyl Hydroperoxide by ZnO-Loaded Single-Atomic Ruthenium Oxide Catalyst," *Journal of the American Chemical Society* 147 (2025): 9134–9146, https://doi.org/10.1021/jacs.4c11685.

10. Y. Jiang, S. Li, Y. Fan, and Z. Tang, "Best Practices for Experiments and Reports in Photocatalytic Methane Conversion," *Angewandte Chemie International Edition* 63 (2025): e202404658, https://doi.org/10.1002/anie.202404658.

11. Y. Cui, W. Zhou, H. Yang, et al., "Largely Promoted C–H Activation in Methane With O_2 via D-Orbital Hybridization Induced by CuO X Supported on ZnO," *ACS Catalysis* 15 (2025): 1607–1615, https://doi.org/10.1021/acscatal.4c06051.

12. P. Wu, Y. Chu, M. Wang, et al., "Subnanometric MoOx Clusters Limit Overoxidation During Photocatalytic CH_4 Conversion to Oxygenates Over TiO_2," *Nature Communications* 16 (2025): 4207, https://doi.org/10.1038/s41467-025-59465-z.

13. Z. Ye, Z. Long, B. Zhang, et al., "Photocatalytic Conversion of Methane to Ethane and Propane Using Cobalt-Cluster-Activated GaN Nanowires," *Angewandte Chemie International Edition* 64 (2025): e202500158, https://doi.org/10.1002/anie.202500158.

14. J. You, Y. Zhang, Z. Wang, et al., "Tuning Reaction Pathway With Surface Metal Cocatalyst for Ethylene Production via Photocatalytic Methane Conversion," *Journal of the American Chemical Society* 147 (2025): 44011–44020, https://doi.org/10.1021/jacs.5c17427.

15. B. Feng, D. Feng, Y. Pei, B. Zong, M. Qiao, and W. Li, "Cu Single Atoms on Defective Carbon Nitride for Photocatalytic Oxidation of Methane to Methanol With Selectivity Over 92%," *Chinese Journal of Catalysis* 76 (2025): 96–107, https://doi.org/10.1016/S1872-2067(25)64730-9.

16. X. Zhang, R. Su, M. Duan, et al., "Ambient Catalyst-free Conversion of Methane to Methanol by Water Radical Cations," *Science Advances* 11 (2025): eadw0584, https://doi.org/10.1126/sciadv.adw0584.

17. F. Si, J. Bai, Y. Li, et al., "Regulating Reactive Oxygen Species via Orbital Rehybridization between Intermediate and Active Site for Selective Methane Photooxidation to Methanol," *Angewandte Chemie International Edition* 64 (2025): e202505267, https://doi.org/10.1002/anie.202505267.

18. R. Tian, S. Fan, G. Chen, and X. Li, "Enzyme-mimetic Functional Synergistic Strategy of Mn-based Spinel Catalysts: Regulating Oxygen Vacancies and Radical Pathways to Promote Photocatalytic Methane Oxidation to C1-C2 Oxygenates," *Applied Catalysis B: Environment and Energy* 382 (2026): 125977, https://doi.org/10.1016/j.apcatb.2025.125977.

19. D. Liu, F. Chen, Y. He, et al., "Intensifying Internal Electric Field on ZnO Nanoplates with Polar Surface Exposure and Cu Doping for Efficient Photocatalytic Methane Oxidation to Oxygenates," *Advanced Functional Materials* 36 (2025): e20271.

20. G. Zhai, S. Yang, Y. Chen, et al., "Direct Photocatalytic Oxidation of Methane to Formic Acid With High Selectivity via a Concerted Proton–Electron Transfer Process," *Journal of the American Chemical Society* 147 (2025): 2444–2454, https://doi.org/10.1021/jacs.4c12758.

21. Y. Wang, Y. Zhang, X. Wang, Y. Liu, and Z. Wu, "Photothermal Direct Methane Conversion to Formaldehyde at the Gas-solid Interface Under Ambient Pressure," *Nature Communications* 16 (2025): 2550, https://doi.org/10.1038/s41467-025-57854-y.

22. M. Sun, Y. Chen, X. Fan, et al., "Electronic Asymmetry of Lattice Oxygen Sites in ZnO Promotes the Photocatalytic Oxidative Coupling of Methane," *Nature Communications* 15 (2024): 9900, https://doi.org/10.1038/s41467-024-54226-w.

23. F. Chen, H. Zhou, D. Liu, et al., "Defective ZnO Nanoplates Supported AuPd Nanoparticles for Efficient Photocatalytic Methane Oxidation to Oxygenates," *Advanced Energy Materials* 14 (2024): 2303642, https://doi.org/10.1002/aenm.202303642.

24. L. Wang, J. Jin, W. Li, et al., "Highly Selective Catalytic Oxidation of Methane to Methanol Using Cu–Pd/Anatase," *Energy & Environmental Science* 17 (2024): 9122–9133, https://doi.org/10.1039/D4EE02671C.

25. H. Li, Q. Shen, Z. Sun, W. Wang, J. Xue, and J. Yu, "Constructing Asymmetric Dual Active Sites through Bimetallic Synergy for Achieving Selective Photocatalytic Nonoxidative Coupling of Methane Toward Ethylene," *ACS Catalysis* 15 (2025): 9717–9727, https://doi.org/10.1021/acscatal.5c01732.

26. R. Zhang, J. Shi, L. Fu, et al., "Direct Photocatalytic Methane Oxidation to Formaldehyde by N Doping Co-Decorated Mixed Crystal TiO_2," *ACS Nano* 18 (2024): 12994–13005, https://doi.org/10.1021/acsnano.4c01318.

27. X. Wang, X. Xin, L. Xiong, et al., "Buffered Hydroxyl Radical for Photocatalytic Non-Oxidative Methane Coupling," *Angewandte Chemie International Edition* 64 (2025): e202420606, https://doi.org/10.1002/anie.202420606.

28. S. Hao, Y. Xue, C. Peng, et al., "Photocatalytic CH_4-to-Ethanol Conversion on Asymmetric Multishelled Interfaces," *Journal of the American Chemical Society* 146 (2024): 25870–25877, https://doi.org/10.1021/jacs.4c08801.

29. Q. Huang, J. Cai, F. Wei, et al., "Selective Oxidative Coupling of Methane to Ethane With Oxygen Using an Au/$Zn_2Ti_3O_8$ Photocatalyst

Under Mild Conditions," *Journal of Materials Chemistry A* 12 (2024): 21334–21340, https://doi.org/10.1039/D4TA02049A.

30. K. Sun, X. Pei, S. Wang, et al., "Synergistic Enhancement of Electron and Hole Transport by Pd Single Atoms and Gradient-Distributed Ti^{3+} Species for High-Performance Photocatalytic Oxidation of CH_4 to Oxygenates," *Angewandte Chemie International Edition* 64 (2025): e202517585, https://doi.org/10.1002/anie.202517585.

31. L. Luo, R. Wang, Z. Wu, et al., "Hydroxyl-Promoted C—C Coupling for Selective Methane Conversion Into Ethane on Cerium Oxide Photocatalyst," *Angewandte Chemie International Edition* 64 (2025): e202510032, https://doi.org/10.1002/anie.202510032.

32. Y. Lei, X. Sala, J. García-Antón, and J. Muñoz, "A Review on Photocatalytic Methane Conversion Systems: From Fundamental Mechanisms to the Emerging Role of Ferroelectric Materials," *Journal of Materials Chemistry A* 13 (2025): 12712–12745, https://doi.org/10.1039/D4TA08554J.

33. K. Yu, Z.-J. Bai, Z. Wang, G. Xie, M. Gonfa, and Z.-J. Wang, "Engineering TiO_2-based Photocatalysts for Selective Methane Conversion: A Critical Review," *Chemical Engineering Science* 320 (2026): 122425, https://doi.org/10.1016/j.ces.2025.122425.

34. S. Han, C. Fan, N. Cheng, et al., "Active Site-Mediated Photo-Thermo Catalysis for Methane Conversion," *Small* 21 (2025): 2503518, https://doi.org/10.1002/smll.202503518.

35. M. A. R. da Silva, C. S. Cunha, L. L. B. Silva, I. G. Farias, and I. F. Teixeira, "Chlorine-mediated Methane Activation: An Efficient Photocatalytic Pathway to Valuable Chemicals," *Chemical Communications* 61 (2025): 3934–3945, https://doi.org/10.1039/D4CC06303A.

36. S. Zhong, D. Yu, Y. Ma, et al., "Oxygen Vacancy-Enhanced Selectivity in Aerobic Oxidation of Benzene to Phenol Over TiO_2 Photocatalysts," *Angewandte Chemie International Edition* 64 (2025): e202502823, https://doi.org/10.1002/anie.202502823.

37. G.-X. Dong, M.-R. Zhang, S.-X. Yuan, M. Zhang, and T.-B. Lu, "Chlorine Radical-Mediated Photocatalytic C—C Coupling of Methanol to Ethylene Glycol With Near-Unity Selectivity," *Angewandte Chemie International Edition* 64 (2025): e202510993, https://doi.org/10.1002/anie.202510993.

38. J. Guo, L. Mao, J. Zhang, and C. Feng, "Role of Cl− Ions in Photooxidation of Propylene on TiO_2 Surface," *Applied Surface Science* 256 (2010): 2132–2137, https://doi.org/10.1016/j.apsusc.2009.09.062.

39. X. Wang, P. Cui, C. Xia, and L. Wu, "Catalytic Boration of Alkyl Halides With Borane Without Hydrodehalogenation Enabled by Titanium Catalyst," *Angewandte Chemie International Edition* 60 (2021): 12298–12303, https://doi.org/10.1002/anie.202100569.

40. B. Ding, T. Liu, W. Zhang, et al., "Synergy of Oxygen Vacancies and Ni Single Atoms Toward Efficient Urea Photosynthesis From CO_2 and N_2," *Angewandte Chemie International Edition* 64 (2025): e202509048, https://doi.org/10.1002/anie.202509048.

41. V.-D. Quach, A. Harsan, M. C. Spadaro, et al., "Oxygen Vacancy Formation at Metal–TiO_2 Interface Yielding Enhanced Photocatalytic Hydrogen Generation," *Advancement of Science* 12 (2025): e01835, https://doi.org/10.1002/advs.202501835.

42. X. Wang, S. Xue, M. Huang, et al., "Pressure-Induced Engineering of Surface Oxygen Vacancies on Metal Oxides for Heterogeneous Photocatalysis," *Journal of the American Chemical Society* 147 (2025): 4945–4951, https://doi.org/10.1021/jacs.4c14073.

43. W. Y. Lim, H. Wu, Y. Lim, and G. W. Ho, "Facilitating the Charge Transfer of $ZnMoS_4$/CuS p–n Heterojunctions Through ZnO Intercalation for Efficient Photocatalytic Hydrogen Generation," *Journal of Materials Chemistry A* 6 (2018): 11416, https://doi.org/10.1039/C8TA02763C.

44. Y.-X. Feng, K. Su, Z.-L. Liu, et al., "A Halide Perovskite Based Ternary Heterojunction With Multi-shell Hollow Structure for Stable and Efficient Artificial Photosynthesis," *Appl Catal B Environ Energy* 347 (2024): 123821, https://doi.org/10.1016/j.apcatb.2024.123821.

45. H. Song, X. Meng, S. Wang, et al., "Direct and Selective Photocatalytic Oxidation of CH_4 to Oxygenates With O_2 on Cocatalysts/ZnO at Room Temperature in Water," *Journal of the American Chemical Society* 141 (2019): 20507–20515, https://doi.org/10.1021/jacs.9b11440.

46. R. Lan, Z. Hu, H. Liu, et al., "Passivating Lattice Oxygen in ZnO Nanocrystals to Reduce Its Interactions With the Key Intermediates for a Selective Photocatalytic Methane Oxidation to Methanol," *Angewandte Chemie International Edition* 64 (2025): e202425186, https://doi.org/10.1002/anie.202425186.

47. X. Sun, T. Yu, Z. Song, Z. Wu, S. An, and Y.-F. Song, "Au Nanoparticles Loaded ZnGaAl-Layered Double Hydroxides for Efficient Photocatalytic Methane Oxidative Coupling," *Advanced Functional Materials* 36 (2026): e11731, https://doi.org/10.1002/adfm.202511731.

48. W. Nie, L. Chen, Y. Hao, et al., "Photocatalytic Oxidative Coupling of Methane to C^{3+} Hydrocarbons via Nanopore-Confined Microenvironments," *Nat Energy* 10 (2025): 1095–1106, https://doi.org/10.1038/s41560-025-01834-5.

49. C.-Y. Huang, J. Li, and C.-J. Li, "A Cross-dehydrogenative C(sp3)—H Heteroarylation via Photo-induced Catalytic Chlorine Radical Generation," *Nature Communications* 12 (2021): 4010, https://doi.org/10.1038/s41467-021-24280-9.

50. C. M. So, S. Kume, and T. Hayashi, "Rhodium-Catalyzed Asymmetric Hydroarylation of 3-Pyrrolines Giving 3-Arylpyrrolidines: Protonation as a Key Step," *Journal of the American Chemical Society* 135 (2013): 10990–10993, https://doi.org/10.1021/ja406169s.

51. G.-X. Dong, M.-R. Zhang, C.-C. Jiao, et al., "Intermarriage of $InVO_4$ and $BiVO_4$ via Cation-Exchange to Boost Charge Separation for Efficient Photocatalytic CH_4 Oxidation to Oxygenates," *Science China Chemistry* 68 (2025): 3807–3815, https://doi.org/10.1007/s11426-024-2536-8.

52. Q. Xiang, J. Yu, and P. K. Wong, "Quantitative Characterization of Hydroxyl Radicals Produced by Various Photocatalysts," *Journal of Colloid & Interface Science* 357 (2011): 163–167, https://doi.org/10.1016/j.jcis.2011.01.093.

53. J. C. Rienstra-Kiracofe, G. S. Tschumper, H. F. Schaefer, S. Nandi, and G. B. Ellison, "Atomic and Molecular Electron Affinities: Photoelectron Experiments and Theoretical Computations," *Chemical Reviews* 102 (2002): 231–282, https://doi.org/10.1021/cr990044u.

54. G. Hippargi, P. Mangrulkar, A. Chilkalwar, N. Labhsetwar, and S. Rayalu, "Chloride Ion: A Promising Hole Scavenger for Photocatalytic Hydrogen Generation," *International Journal of Hydrogen Energy* 43 (2018): 6815–6823, https://doi.org/10.1016/j.ijhydene.2017.12.179.

Supporting Information

Additional supporting information can be found online in the Supporting Information section.

Supporting File: anie72726-sup-0001-SuppMat.docx.